Structural Engineering and Mechanics, Vol. 14, No. 5 (2002) 521-542
DOI: http://dx.doi.org/10.12989/sem.2002.14.5.521

Structural vibration control using resistively shunted piezoceramics

S.B. Kandagal† and Kartik Venkatraman‡

Aeroservoelasticity Laboratory, Department of Aerospace Engineering, Indian Institute of Science, Bangalore 560 012, India

(Received July 13, 2001, Accepted August 16, 2002)

Abstract. Application of piezoceramic materials in actuation and sensing of vibration is of current interest. Potential and more popular applications of piezoceramics are probably in the field of active vibration control. However, the objective of this work is to investigate the effect of shunted piezoceramics as passive vibration control devices when bonded to a host structure. Resistive shunting of a piezoceramic bonded to a cantilevered duralumin beam has been investigated. The piezoceramic is connected in parallel to an electrical network comprising of resistors and inductors. The piezoceramic is a capacitor that stores and discharges electrical energy that is transformed from the mechanical motion of the structure to which it is bonded. A resistor across the piezoceramic would be termed as a resistively shunted piezoceramic. Similarly, an inductor across the piezoceramic is termed as a resonantly shunted piezoceramic. In this study, the effect of resistive shunting on the nature of damping enhancement to the host structure has been investigated. Analytical studies are presented along with experimental results.

Key words: vibration control; piezoceramic; resistive shunting.

1. Introduction

Piezoceramic materials are transformers that convert mechanical energy to electrical energy and *vice-versa*. Conventional applications of these materials are as actuators to generate vibration or acoustic waves, or sensors that convert mechanical motion and acoustic disturbances to electrical signals. However, the very idea of a transformer that converts mechanical energy into electrical energy gives rise to possibilities of controlling mechanical motion.

When these piezoceramics are bonded to a structure, the mechanical strain energy generated in the piezoceramic is converted to electrical voltage across the poling direction of the piezoceramic device. This voltage or electrical energy is dissipated or shunted to another frequency band using electrical networks connected to the terminals of the piezoceramic as shown in Fig. 1. The mechanical energy of motion of the structure is thereby controlled.

Note that if the electrical networks contain electrical energy sources, then we term the network as an active network, and the control scheme as an active control one. If there are no energy sources in the electrical network, then the network is known as a passive network, and the control scheme a

† Graduate Student
‡ Assistant Professor

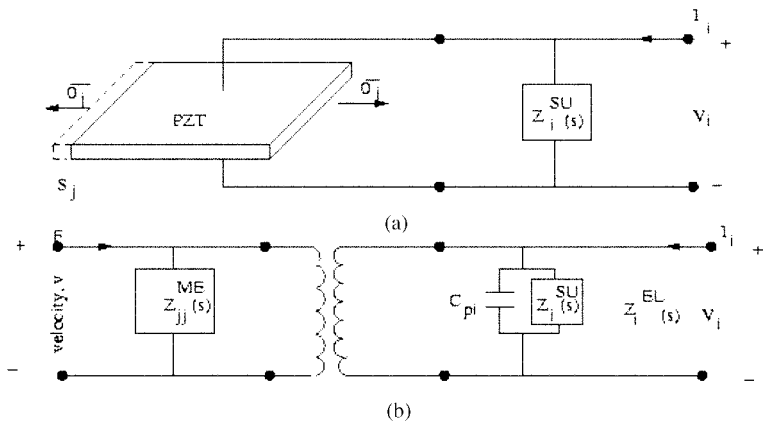

Fig. 1 (a) Physical model of uniaxial shunted piezoelectric, (b) network analog

passive control one. The present work will be concerned with the latter.

Passive vibration absorbers, or controllers, are well known in vibration engineering (Mallik 1990, Harris 1996). Most of these passive controllers have limited tuning capability to adapt to different operating regimes in which the dynamical system is likely to be subjected, such as changes in external excitation frequency or amplitude, and even change in system parameters. This is one of the reasons for the move towards active vibration control devices. However, piezoceramic materials with tunable passive electrical networks are essentially passive vibration controllers that can be tuned to cope with varied operating conditions. The tunable passive electrical networks connected to the piezoceramic can modify the frequency selective vibration transmission properties of the structure itself.

It is important to note that a mechanical system is a frequency selective filter, with pass-bands and stop-bands, and thus any vibration control device whether active or passive, essentially modifies the frequency selective filtering capabilities of the mechanical system.

Electrical passive shunting of piezoceramics has been investigated in the recent past (Hagood and von Flotow 1991, Davis and Lesieutre 1995). These studies have focused on experimental investigation of the additive damping and change in resonance frequency. The analytic vibration models represent the damping and stiffness due to electrical shunting of the piezoceramic as a complex frequency dependent modulus similar to that used in viscoelastic solids (Hagood and von Flotow 1991). The optimum shunting parameters for the piezoceramic vibration absorber is also derived and experimentally verified.

The subject of the present work is in a sense complementary to that of Hagood and von Flotow (1991). The dynamic characteristic of a vibrating system that has piezoceramic layer bonded onto it is studied with resistive shunting. Besides confirming the experimental and analytical results obtained by Hagood and von Flotow (1991), the present work investigates the effect of thickness and length ratios of the piezoceramic with reference to the host beam structure in changing the damping loss factors and resonance frequencies. Results are also presented for the vibration reduction in the first two modes of a cantilevered beam using resistively shunted piezoceramics. The most suitable location of the piezoceramic in effecting this vibration reduction is also discussed. Further, in order to investigate the presence of any nonlinearity due to the piezoceramic as well as

resistive shunting, the effect of vibration amplitude and excitation frequency on the loss factor is also investigated.

2. Modeling of shunted piezoceramic materials

The constitutive equations of a linear piezoelectric material can be written as Hagood and von Flotow (1991)

$$\begin{bmatrix} \boldsymbol{q} \\ \boldsymbol{\varepsilon} \end{bmatrix} = \begin{bmatrix} \boldsymbol{E} & \boldsymbol{D} \\ \boldsymbol{D}^T & \boldsymbol{C}^{SC} \end{bmatrix} \begin{bmatrix} \Phi \\ \sigma \end{bmatrix} \tag{1}$$

where the electric displacement, mechanical strain, electric field, and mechanical stress, are defined, respectively, as:

$$\begin{aligned} \boldsymbol{q} &= [q_1, q_2, q_3]^T \\ \boldsymbol{\varepsilon} &= [\varepsilon_{11}, \varepsilon_{22}, \varepsilon_{33}, 2\varepsilon_{23}, 2\varepsilon_{13}, 2\varepsilon_{12}]^T \\ \Phi &= [\Phi_1, \Phi_2, \Phi_3]^T \\ \sigma &= [\sigma_{11}, \sigma_{22}, \sigma_{33}, \sigma_{23}, \sigma_{13}, \sigma_{12}]^T \end{aligned} \tag{2}$$

The piezo dielectric constant matrix $\boldsymbol{E}$, piezoelectric electromechanical coupling matrix $\boldsymbol{D}$ and mechanical compliance matrix $\boldsymbol{C}^{SC}$, are expressed, respectively, as:

$$\boldsymbol{E} = \begin{bmatrix} e_{01} & 0 & 0 \\ 0 & e_{01} & 0 \\ 0 & 0 & e_{03} \end{bmatrix} \tag{3}$$

$$\boldsymbol{D} = \begin{bmatrix} 0 & 0 & 0 & 0 & d_{15} & 0 \\ 0 & 0 & 0 & d_{15} & 0 & 0 \\ d_{31} & d_{31} & d_{33} & 0 & 0 & 0 \end{bmatrix} \tag{4}$$

$$\boldsymbol{C}^{SC} = \begin{bmatrix} c_{11}^{SC} & c_{12}^{SC} & c_{13}^{SC} & 0 & 0 & 0 \\ c_{12}^{SC} & c_{11}^{SC} & c_{13}^{SC} & 0 & 0 & 0 \\ c_{13}^{SC} & c_{13}^{SC} & c_{33}^{SC} & 0 & 0 & 0 \\ 0 & 0 & 0 & c_{55}^{SC} & 0 & 0 \\ 0 & 0 & 0 & 0 & c_{55}^{SC} & 0 \\ 0 & 0 & 0 & 0 & 0 & c_{66}^{SC} \end{bmatrix} \tag{5}$$

In the above, the superscript *SC* indicates the value of the mechanical compliance with short circuit boundary condition or constant electric field.

Representing these equations in terms of voltages and currents, where the voltages and currents are defined respectively as:

$$v_i = \int_0^{L_i} \Phi_i dx_i, \qquad i_i = \int_{A_i} q_i da_i \tag{6}$$

Assuming that the field within, and electrical charge on the surface, is uniform for the piezoelectric material, relations (6) become, in the Laplace domain, as:

$$\boldsymbol{v}(s) = \boldsymbol{L}\Phi(s) \qquad \boldsymbol{i}(s) = s\boldsymbol{A}\boldsymbol{q}(s) \tag{7}$$

where $\boldsymbol{L}$ is a diagonal matrix whose elements are the lengths of the piezoceramic patch in the ith direction, $\boldsymbol{A}$ is the diagonal matrix whose elements are the areas of surfaces perpendicular to the ith direction, and s is the Laplace parameter. By taking the Laplace transform of Eq. (1), and using Eq. (7) to eliminate $\boldsymbol{\Phi}$ and $\boldsymbol{q}$, the general equation for a piezoelectric in terms of the external current input and applied voltage is obtained as:

$$\begin{bmatrix} \boldsymbol{i} \\ \boldsymbol{\varepsilon} \end{bmatrix} = \begin{bmatrix} s\boldsymbol{A}\boldsymbol{E}\boldsymbol{L}^{-1} & s\boldsymbol{A}\boldsymbol{D} \\ \boldsymbol{D}^T\boldsymbol{L}^{-1} & \boldsymbol{C}^{SC} \end{bmatrix} \begin{bmatrix} \boldsymbol{v} \\ \boldsymbol{\sigma} \end{bmatrix} \tag{8}$$

The generalized compliance matrix in the upper left partition is diagonal and the elements of this partition have the form,

$$A_i E_i / L_i = C_{pi} \tag{9}$$

where C_{pi} is the capacitance between the surfaces perpendicular to the ith direction at constant stress. By grouping these into $\boldsymbol{C}_p$ the constituent relations, Eq. (8), becomes,

$$\begin{bmatrix} \boldsymbol{i} \\ \boldsymbol{\varepsilon} \end{bmatrix} = \begin{bmatrix} s\boldsymbol{C}_p & s\boldsymbol{A}\boldsymbol{D} \\ \boldsymbol{D}^T\boldsymbol{L}^{-1} & \boldsymbol{C}^{SC} \end{bmatrix} \begin{bmatrix} \boldsymbol{v} \\ \boldsymbol{\sigma} \end{bmatrix} = \begin{bmatrix} \boldsymbol{Y}^{OC}(s) & s\boldsymbol{A}\boldsymbol{D} \\ \boldsymbol{D}^T\boldsymbol{L}^{-1} & \boldsymbol{C}^{SC} \end{bmatrix} \begin{bmatrix} \boldsymbol{v} \\ \boldsymbol{\sigma} \end{bmatrix} \tag{10}$$

where $\boldsymbol{Y}^{OC}(s)$ is the open circuit admittance of the piezoelectric. For shunted piezoelectric applications, a passive electrical circuit is connected between the surface electrodes, as shown in Fig. 1. Since the circuit is placed across the electrodes, it appears in parallel to the inherent piezoelectric capacitance in that direction. The admittances add in parallel. Hence the governing constitutive Eq. (10) becomes,

$$\begin{bmatrix} \boldsymbol{i} \\ \boldsymbol{\varepsilon} \end{bmatrix} = \begin{bmatrix} \boldsymbol{Y}^{EL} & s\boldsymbol{A}\boldsymbol{D} \\ \boldsymbol{D}^T\boldsymbol{L}^{-1} & \boldsymbol{C}^{SC} \end{bmatrix} \begin{bmatrix} \boldsymbol{v} \\ \boldsymbol{\sigma} \end{bmatrix} \tag{11}$$

where

$$\boldsymbol{Y}^{EL} = \boldsymbol{Y}^{SC} + \boldsymbol{Y}^{SU} \tag{12}$$

The externally applied current, $\boldsymbol{i}$ is the sum of the currents flowing through the shunting impedance, the inherent piezoelectric capacitance, and the piezoelectric transformer (Fig. 1). The shunting admittance matrix is assumed to be diagonal and frequency dependent, that is,

$$\boldsymbol{Y}^{SU}(s) = \begin{bmatrix} \boldsymbol{Y}_1^{SU}(s) & 0 & 0 \\ 0 & Y_2^{SU}(s) & 0 \\ 0 & 0 & Y_3^{SU}(s) \end{bmatrix} \tag{13}$$

The superscript SU indicates the shunted value. The voltage appearing across the electrodes can be estimated from Eq. (11), which will be

$$v = (\boldsymbol{Z}^{EL})\boldsymbol{i} - (\boldsymbol{Z}^{EL})s\boldsymbol{A}\boldsymbol{D}\sigma \tag{14}$$

where $\boldsymbol{Z}^{EL}$ is the electrical impedance matrix and is equal to $(\boldsymbol{Y}^{EL})^{-1}$**.** The strains in terms of stress and input current can be obtained by substituting Eq. (14) in Eq. (11),

$$\varepsilon = [\boldsymbol{C}^{SC} - \boldsymbol{D}^T\boldsymbol{L}^{-1}\boldsymbol{Z}^{EL}s\boldsymbol{A}\boldsymbol{D}]\sigma + [\boldsymbol{D}^T\boldsymbol{L}^{-1}\boldsymbol{Z}^{EL}]\boldsymbol{i} \tag{15}$$

This governing equation for the shunted piezoelectric gives the strain for a given applied stress and forcing current. The shunted piezoelectric compliance can be defined from Eq. (15), as

$$\boldsymbol{C}^{SU} = [\boldsymbol{C}^{SC} - \boldsymbol{D}^T\boldsymbol{L}^{-1}\boldsymbol{Z}^{EL}s\boldsymbol{A}\boldsymbol{D}] \tag{16}$$

It is to be noted that the short circuit electrical impedance and open circuit electrical impedance at constant stress will be, $\boldsymbol{Z}^{SC}(s) = \boldsymbol{0}$ and $\boldsymbol{Z}^{OC}(s) = (s\boldsymbol{C}_p)^{-1}$, respectively, where

$$s\boldsymbol{C}_p = s\boldsymbol{L}^{-1}\boldsymbol{E}\boldsymbol{A} \tag{17}$$

Eq. (16) can be now rewritten as

$$\boldsymbol{C}^{SU} = [\boldsymbol{C}^{SC} - \boldsymbol{D}^T\overline{\boldsymbol{Z}}^{EL}\boldsymbol{E}^{-1}\boldsymbol{D}] \tag{18}$$

where the non-dimensional electrical impedance matrix is defined as

$$\overline{Z}^{EL} = \boldsymbol{Z}^{EL}(\boldsymbol{Z}^{OC})^{-1} = (s\boldsymbol{C}_p + \boldsymbol{Y}^{SU})^{-1}s\boldsymbol{C}_p \tag{19}$$

Since $\overline{\boldsymbol{Z}}^{EL}$ is diagonal, the electrical contribution to the compliance can be written as the summation of electrical impedances,

$$\boldsymbol{C}^{SU} = \left[\boldsymbol{C}^{SC} - \sum_{i=1}^{3} \overline{Z}_i^{EL}\left[\left(\frac{\boldsymbol{D}^T}{\boldsymbol{D}_i}\boldsymbol{E}_i^T\right)\right]\right] = \left[\boldsymbol{C}^{SC} - \sum_{i=1}^{3} \overline{Z}_i^{EL}M_i\right], \tag{20}$$

where $\boldsymbol{D}_i$ denotes i^{th} row of $\boldsymbol{D}$, and for piezoceramics, the $\boldsymbol{M}_i$ have the form

$$\boldsymbol{M}_1 = \frac{1}{e_{01}}\begin{bmatrix} 0 & 0 & 0 & 0 & 0 & 0 \\ 0 & 0 & 0 & 0 & 0 & 0 \\ 0 & 0 & 0 & 0 & 0 & 0 \\ 0 & 0 & 0 & 0 & 0 & 0 \\ 0 & 0 & 0 & 0 & d_{15}^2 & 0 \\ 0 & 0 & 0 & 0 & 0 & 0 \end{bmatrix}$$

$$\boldsymbol{M}_2 = \frac{1}{e_{01}}\begin{bmatrix} 0 & 0 & 0 & 0 & 0 & 0 \\ 0 & 0 & 0 & 0 & 0 & 0 \\ 0 & 0 & 0 & 0 & 0 & 0 \\ 0 & 0 & 0 & d_{15}^2 & 0 & 0 \\ 0 & 0 & 0 & 0 & 0 & 0 \\ 0 & 0 & 0 & 0 & 0 & 0 \end{bmatrix}$$

$$\boldsymbol{M}_3 = \frac{1}{e_{03}}\begin{bmatrix} d_{31}^2 & d_{31}^2 & d_{31}d_{33} & 0 & 0 & 0 \\ d_{31}^2 & d_{31}^2 & d_{31}d_{33} & 0 & 0 & 0 \\ d_{31}d_{33} & d_{31}d_{33} & d_{33}^2 & 0 & 0 & 0 \\ 0 & 0 & 0 & 0 & 0 & 0 \\ 0 & 0 & 0 & 0 & 0 & 0 \\ 0 & 0 & 0 & 0 & 0 & 0 \end{bmatrix} \tag{21}$$

The above equations constitute the expression for the compliance matrix of a piezoelectric element. Eq. (20) can be simplified further, when the piezoelectric element is loaded uniaxially with either a normal or shear stress, with only one pair of electrodes to provide an external electric field in only one direction. For loading in the jth direction and the field in the ith direction, the shunted compliance will be:

$$C_{jj}^{SU} = C_{jj}^{SC} - \bar{Z}_i^{EL}(d_{ij}^2)/e_{0i} \tag{22}$$

Further study of the effectiveness of electrical shunting of a piezoceramic in controlling vibration requires that we define a quantity known as the electromechanical coupling coefficient. It is defined as the ratio of the peak energy stored in the capacitor to the peak energy stored in the material due to mechanical strain with the piezoelectric electrodes short-circuited. It represents the percentage of mechanical strain energy that is converted into electrical energy and *vice-versa*. The piezoceramic material electromechanical coupling coefficient, k_{ij} is defined as:

$$k_{ij} = d_{ij}\sqrt{C_{jj}^{SC} e_{0i}} \tag{23}$$

The compliance C_{jj}^{SU} is obtained by substituting Eq. (23) in Eq. (22),

$$C_{jj}^{SU} = C_{jj}^{SC}(1 - k_{ij}^2 \overline{Z}_i^{EL}) \tag{24}$$

The compliance of the shunted piezoelectric is equal to the short circuit compliance of the piezoelectric material modified by a non-dimensional term that depends on the electrical shunting circuit and the material's electromechanical coupling coefficient. Substituting $\overline{Z}^{EL} = 1$, for the open circuit case, we get the open-circuit mechanical compliance as,

$$C_{jj}^{OC} = C_{jj}^{SC}[1 - k_{ij}^2] \tag{25}$$

In Eq. (25), *OC* denotes the value taken with open circuit boundary conditions (constant charge) and it can be observed from Eq. (25) that the change in mechanical properties of the piezoceramic as the piezoceramic electric boundary conditions are changed from short circuit to open circuit.

The mechanical impedance of the shunted piezoceramic can be obtained in the non-dimensional form by using Eqs. (24) and (25). For uniaxial loading in the jth direction, the mechanical impedance of the piezoelectric can be expressed as a function of the Laplace parameter, s, as

$$Z_{jj}^{ME}(s) = \frac{A_j}{C_{jj}^{SU} L_j s} \tag{26}$$

The superscript *ME* refers to the mechanical property in the system. The final expression for the non-dimensional mechanical impedance, which is defined as the ratio of the shunted mechanical impedance to the open circuit impedance, for the shunted piezoelectric, can be derived using Eq. (26) and Eq. (24) as

$$\overline{Z}_{jj}^{ME} = \frac{Z_{jj}^{SU}(s)}{Z_{jj}^{OC}(s)} = \frac{(1 - k_{ij}^2)}{[1 - k_{ij}^2 \overline{Z}_{jj}^{EL}(s)]} \tag{27}$$

Note that the non-dimensional mechanical impedance, $\overline{Z}_{jj}^{ME}$, is in general complex and frequency dependent since it depends on the frequency dependent complex electrical impedance. This complex mechanical impedance can be represented in the familiar way as,

$$\overline{Z}_{jj}^{ME} = \overline{E}_{jj}(\omega)[1 + i\eta_{jj}(\omega)] \tag{28}$$

where $\overline{Z}_{jj}$ is the ratio of shunted stiffness to open circuit stiffness of the piezoelectric, and η_{jj} is the material loss factor. This leads to frequency dependent equations for the complex modulus of the shunted piezoelectric. The loss factor η and modulus E can be expressed as

$$\eta_{jj}(\omega) = \frac{Im[\overline{Z}^{ME}(s)]}{Re[\overline{Z}^{ME}(s)]}, \qquad \overline{E}_{jj}(\omega) = Re[\overline{Z}^{ME}(s)] \tag{29}$$

For the case when resistors are used as shunting devices, as shown in Fig. 2, the resistor acts as an energy dissipater on the electrical side. As discussed above, electrical shunting of a piezoceramic bonded to a host structure is equivalent to a viscoelastic damping treatment of the same host structure.

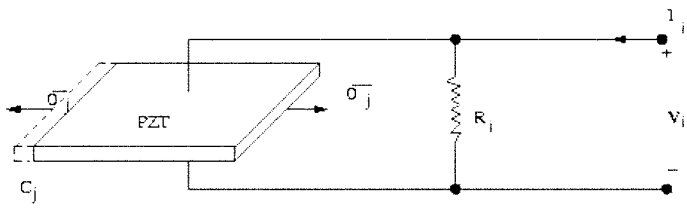

Fig. 2 Resistive shunting of piezoceramic

The non-dimensional mechanical impedance of a resistive shunted piezoelectric, using Eq. (27) and Eq. (19), is given by

$$Z_i^{SU}(s) = R_i, \qquad \bar{Z}_i^{EL}(s) = \frac{Z_i^{EL}(s)}{Z_i^{OC}(s)} = \frac{sC_{pi}R_i}{1 + sC_{pi}R_i} \tag{30}$$

$$\bar{Z}_{jj}^{RES}(\omega) = 1 - \frac{k_{ij}^2}{1 + i\rho_i} \tag{31}$$

The superscript *RES* relates to the resistive shunting, where $\boldsymbol{R}_i$ is the resistance across the piezoceramic, and ρ_i is the non-dimensional frequency defined as

$$\rho_i = R_i C_{pi}\omega \tag{32}$$

Eq. (31) is the frequency dependent mechanical impedance of the vibrating structure with resistively shunted piezoceramic bonded to it. The loss factor and the frequency dependent storage modulus are, in terms of Eqs. (28) and (29), respectively,

$$\eta_{jj}^{RES}(\omega) = \frac{\rho_i k_{ij}^2}{(1 - k_{ij}^2) + \rho_i^2} \tag{33}$$

$$\bar{E}_{jj}^{RES}(\omega) = 1 - \frac{k_{ij}^2}{(1 + \rho_i^2)} \tag{34}$$

The behavior of material loss factor and stiffness ratio as a function of non-dimensional frequency (or non-dimensional resistance), for various values of k_{31} is shown in Fig. 3 and Fig. 4. These curves are similar to that of a linear viscoelastic solid (Mallik 1990, Nashif *et al.* 1985). In Fig. 3, for a given resistance, the material loss factor of the resistively shunted piezoceramic changes from its short circuit value at low frequencies to its open circuit value at high frequencies. The material exhibits a maximum loss factor equal to

$$\eta_{\max}^{RES} = \frac{k_{ij}^2}{2\sqrt{(1 - k_{ij}^2)}} \tag{35}$$

at a non-dimensional frequency

$$\rho_i = R_i C_{pi}\omega = \sqrt{(1 - k_{ij}^2)} \tag{36}$$

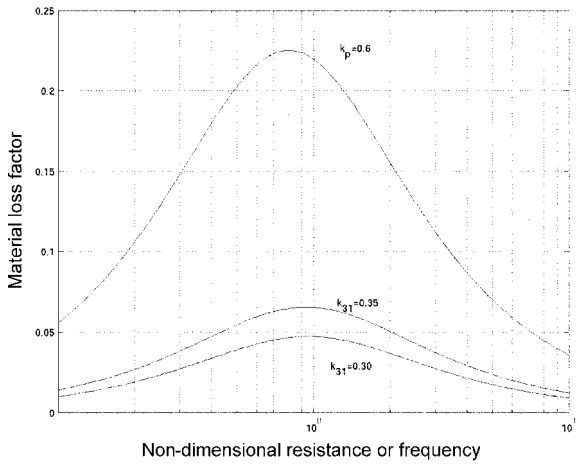

Fig. 3 Variation of material loss factor of a resistively shunted piezoelectric in transverse case for different k_{31}

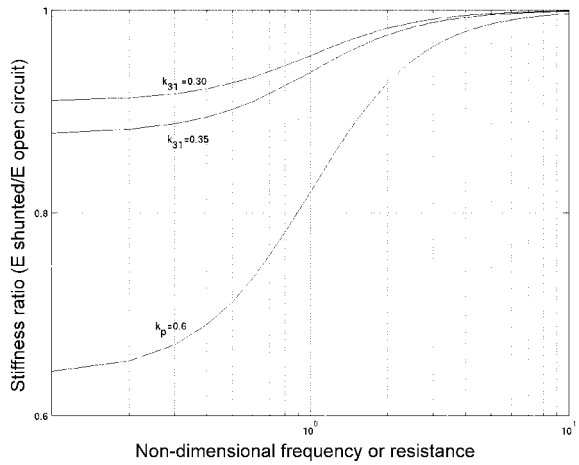

Fig. 4 Variation of storage modulus of a resistively shunted piezoelectric in transverse case for different k_{31}

Fig. 4 represents the variation of the non-dimensional stiffness, that is the ratio of the resistively shunted piezoceramic stiffness to the open-circuit piezoceramic stiffness, as a function of non-dimensional frequency or resistance. For a given resistance value, this ratio varies from the short-circuit value at low frequencies to the open-circuit value at high frequencies.

In view of Eq. (32), Fig. 3 and Fig. 4 can also be interpreted as the variation of the loss factor and non-dimensional stiffness as a function of the resistive load in the shunting circuit. In this case, the frequency of vibration is kept fixed and only the resistance is varied.

Fig. 3 and Fig. 4, also show the effect of electromechanical coupling coefficient k_{31} on the loss factor and stiffness. Higher k_{31} ensures higher added damping and stiffness. A maximum k_{31} value of 0.36 can be realized with current generation of commercially available piezoceramic materials. Although values of k_{31} greater than 0.36 is not presently attainable, k_p (planar electromechanical coupling coefficient) and k_{33} values in the range of 0.6 are attainable with currently manufactured piezoceramics. As shown in Fig. 3, the additive loss factor due to resistive shunting can be as high as 25% for the case when $k_p = 0.6$. A similar trend presents itself in the case of stiffness ratio as shown in Fig. 4. It is to be noted that vibration control through piezoceramic shunting is not only tunable, but also does not suffer from rubber-to-glass transition problems associated with viscoelastic materials.

In order to study the effectiveness of piezo-resistive shunting in controlling the dynamics of a vibrating system, the dynamics of the host structure is modeled by a single vibration mode. The piezoceramic is then coupled in parallel to this one degree-of-freedom (1-DOF) system as shown in Fig. 5. The modal velocity of the vibrating system with piezoceramic can be expressed in the Laplace domain as

$$v(s) = \frac{F(s)}{Ms + (K/s) + Z_{jj}^{RES}(s)} \tag{37}$$

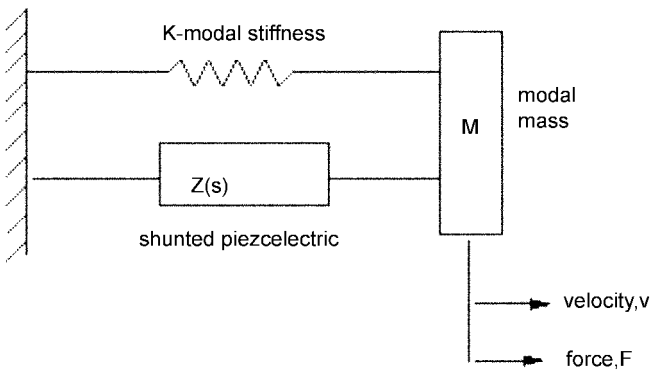

Fig. 5 Sdof system model with shunted piezoelectric element in parallel with the system modal mass

where *Ms* is the impedance associated with modal mass of the host structure, *K/s* is the impedance associated with the modal stiffness of the host structure, and $Z_{jj}^{RES}(s)$ is the impedance associated with the resistively shunted piezoceramic.

The transfer function for the mechanical system shown in Fig. 5 can be expressed as follows:

$$\frac{x}{x^{ST}} = \frac{(r\gamma + 1)}{(r\gamma^3 + \gamma^2 + r(1 + K_{ij}^2)\gamma + 1)} \tag{38}$$

where, x^{ST} represents F/K_{tot}, and K_{tot} is the sum of base system modal stiffness and the piezoelectric short-circuit modal stiffness.

The non-dimensional frequency and electrical damping ratio are, respectively,

$$\gamma = s/\omega_n^{SC}$$
$$r = R_i C_{pi} \omega_n^{SC} \tag{39}$$

where the system natural frequency (with the piezoceramic shorted) is

$$\omega_n^{SC} = \sqrt{(K + K_{pzt})/M} \tag{40}$$

and K_{pzt}, is the short-circuit stiffness of the piezoceramic. K and M are the system modal stiffness and modal mass respectively. We can define a generalized mechanical coupling coefficient K_{ij} such that

$$K_{ij}^2 = \left(\frac{K_{pzt}}{K + K_{pzt}}\right)\left(\frac{k_{ij}^2}{1 - k_{ij}^2}\right) \tag{41}$$

The generalized electromechanical coupling coefficient K_{ij} is a measure of the overall conversion of electrical energy into mechanical energy by the piezoceramic, when it is short-circuited, and coupled to a host structure. Note that it is different from the material electromechanical coupling coefficient, k_{31}, in that, K_{31} accounts for the effect of the host structure on the piezoceramic transformer's electro-mechanical conversion efficiency.

The above modeling of the resistively shunted piezoceramic bonded to the host structure assumes a linear electro-mechanical coupling leading to a linear viscoelastic model of the overall structural dynamics.

We next outline the experimental set-up to validate the analytical predictions made above. Numerical simulations of the analytical results are compared with experimentally obtained results for the test-specimen.

3. Experimental set-up

In order to investigate the dynamic behavior of the resistively shunted piezoceramic bonded to a structure, dynamic tests were conducted on two duralumin cantilever beam specimens with surface bonded piezoceramic patches. The first cantilever beam specimen (Beam-I) was 166 mm long, 30.5 mm wide, and 0.9 mm thick, where as the second beam (Beam-II) was 250 mm long, 26 mm wide and 1.5 mm thick. Both are shown in Fig. 6 and Fig. 7. The piezoceramic patches were attached to the beam with a very thin layer of epoxy. The material properties of the beam and

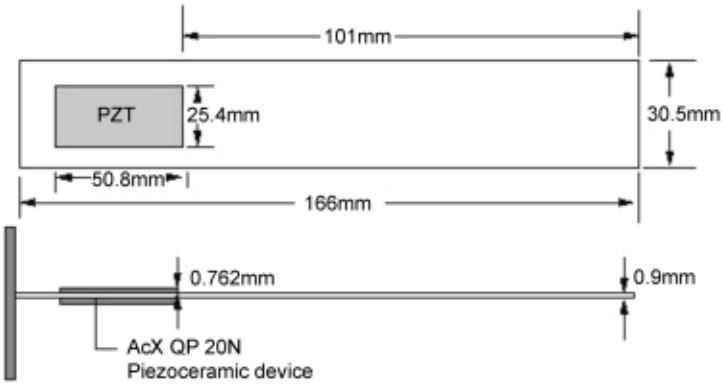

Fig. 6 Beam-I with PZT

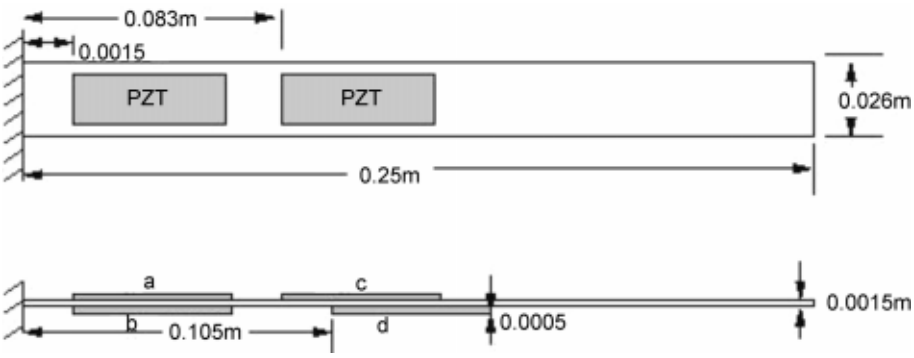

Fig. 7 Beam-II with PZT

Table 1 Cantilever beam and PZT dimensions and properties

Material	Duralumin	Duralumin	PZT	PZT
Property	Beam-I	Beam-II	AcX	Sparkler
Length (mm)	166	250	50.8	50
Width (mm)	30.5	26	25.4	25
Thickness (mm)	0.9	1.5	0.762	0.5
E (GPa)	70	70	69	69
Capacitance (μF)	-	-	0.09	0.06
Density (kg/m^3)	2700	2700	7700	7800
Coupling coefficient (k_{31})	-	-	0.30	0.35

piezoceramic are listed in Table 1.

Dynamic tests were conducted on the bare duralumin model to determine the baseline vibration characteristics such as the resonance frequencies, modal damping, and the mode shapes of the beam without PZT.

For all the vibration tests with electrically shunted piezoceramics, the shunting resistance was varied between 0-1000 kΩ. The natural frequencies of the beam were found using impulse excitation technique consisting of an instrumented impulse hammer model PCB Piezotronics 208A03, B&K 4344 accelerometer, and B&K 2635 charge amplifier.

The experimental setup is shown in Fig. 8. The beam was excited at its first two resonance frequencies using Derritron VP2MM exciter, 25W Derritron power amplifier, and A&D AD-3525 signal generator. Input force was measured using B&K 8200 force transducer and amplified by B&K 2626 conditioning amplifier.

The acceleration response of the beam was picked up near the tip by B&K 4344 accelerometer and amplified by B&K 2635 charge amplifier. These signals were acquired by National Instruments ATMIO 16 data acquisition card using LabView (Ver.5.0) software. Constant input force level was ensured throughout the experiment.

Damping was estimated from the energy dissipated in one cycle. The area enclosed within the force-displacement curve for the vibrating system with piezo bonded to it gives this. That is,

$$U = \oint F dx = \int_0^{2\pi/\Omega} F v dt \tag{42}$$

where Ω is the excitation frequency and $v(t)$ is the velocity.

Displacement and velocity signals were obtained by integrating successively the acceleration signal using high-pass Butterworth filters implemented in Matlab/Simulink (Ver.5.3(R11)) as shown in Fig. 9. These filters are needed to remove the constant of integration that appears in the integrated signal as a DC bias term. The filter order and cut-off frequency need to be chosen with care since they can phase distort the integrated signal. To prevent phase distortion, the phase of the acceleration, velocity and displacement signals were checked so that they successively lagged each other by 90° (Kandagal *et al.* 2001).

To compare the damping performance of shunted PZT, equivalent damping coefficient C_{eqv} was evaluated using the relation

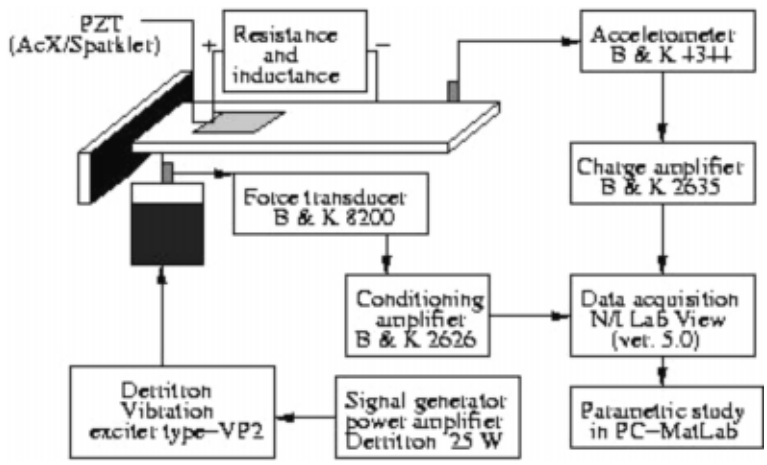

Fig. 8 Experimental setup

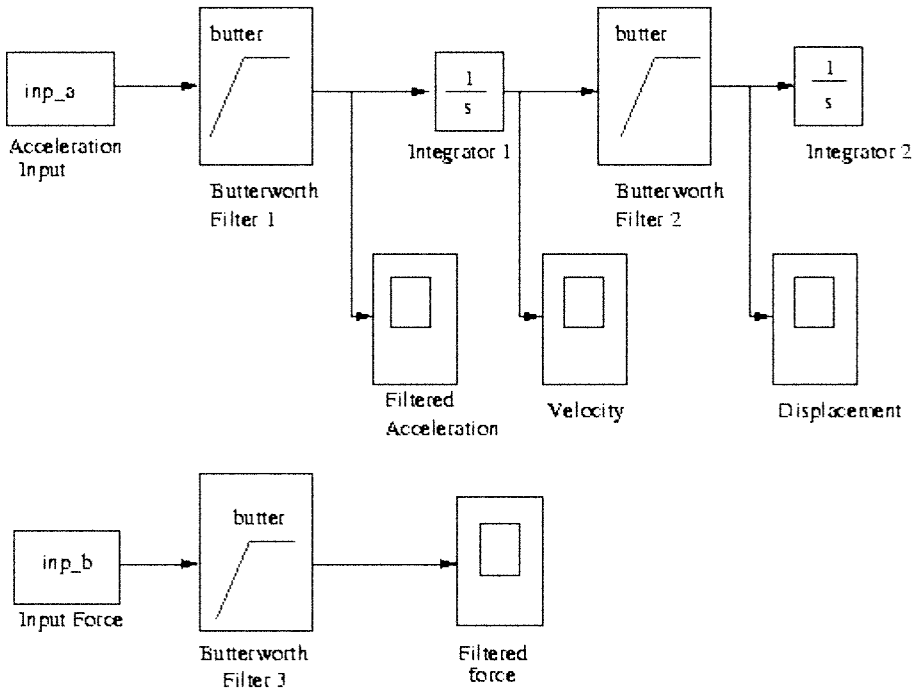

Fig. 9 Filter characteristics

$$C_{eqv} = \frac{U}{\pi \Omega X_0^2} \tag{43}$$

where U is the energy dissipated in one cycle, given by Eq. (42), X_o is the displacement amplitude, and Ω is the frequency of excitation. C_{eqv} is evaluated for different resistance values. The damping ratio, ζ, follows as:

$$\zeta = \frac{C_{eqv}}{2\omega_n} \tag{44}$$

The excitation frequency in all the experiments was set equal to the one of the first two resonance frequencies.

4. Discussion of results

We conducted resistive shunting experiments with piezos bonded to two beams with different thickness. The motivation was also to investigate the effect of thickness ratio on resistive shunting. We first present results for Beam-I, the thinner beam, and subsequently for Beam-II.

4.1 Beam-I

The frequency response test results for Beam-I, shown in Fig. 6, using instrumented impulse hammer, are presented in Table 2. The natural frequencies of the beam with piezo short- and open-circuited are the same. Analytically predicted difference between the open and short circuit resonance frequencies is shown in Fig. 10. The shift in the natural frequency is beyond the least-count of the FFT analyzer (equal to 0.0625 Hz). Hence, change in the natural frequencies of the beam with piezo short and open circuited was not observed. Indeed, this experimental observation is discussed in more detail below together with numerical simulations.

K_{pzt}, appearing in Eq. (40), was determined using the procedure outlined in Crawley and de Luis (1987).

The added damping due to resistive shunting was evaluated from Eq. (38). The value of the electromechanical coupling coefficient, k_{ij}, as given by the manufacturer, is equal to 0.3. As discussed earlier, Fig. 3 and Fig. 4 show the variation in loss factor and stiffness of the piezoceramic alone with variation in resistance. In order to study the effectiveness of resistive shunting of the piezoceramic on vibration control of the structure, we evaluated the response transfer function as given by Eq. (38). Note that rather than k_{ij}, it is the generalized electromechanical coupling coefficient, K_{ij}, that is critical. K_{ij} evaluated from Eq. (41), and using the value of $k_{ij} = 0.3$, is 0.12.

Table 2 Experimentally measured parameters for resistive shunting

Parameters	Beam-I	Beam-II	Beam-II
Mode	I	I	II
Natural frequency without PZT	16.8 Hz	18 Hz	97 Hz
Natural frequency (PZT-shorted)	22.5 Hz	21 Hz	105 Hz
Natural frequency (PZT-open)	22.5 Hz	21.32 Hz	105.4 Hz
Loss factor (without PZT)	0.0016	0.0058	0.0034
Loss factor (with PZT short circuited)	0.0078	0.0214	0.011
Generalized coupling coefficient (estimated) K_{ij}	0.04	0.165	0.0127
Generalized coupling coefficient (measured) K_{ij}	0.035	0.153	0.11
Capacitance	0.09 μF	0.06 μF	0.06 μF
Optimal resistance	70 kΩ	110 kΩ	25 kΩ
Non-dimensional resistance	0.9	0.9	0.9

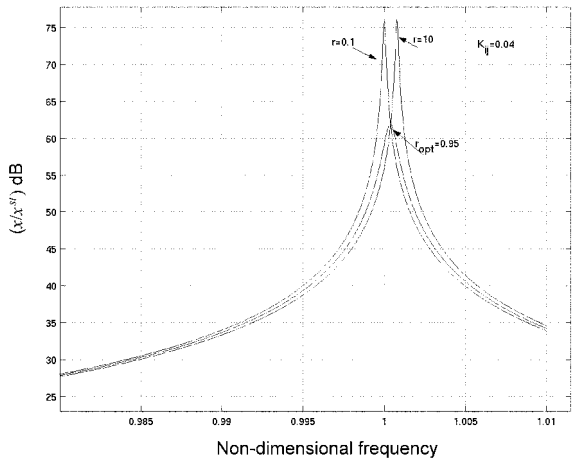

Fig. 10 Response of 1-DOF system with resistively shunted piezoelectric; $K_{ij} = 0.12$

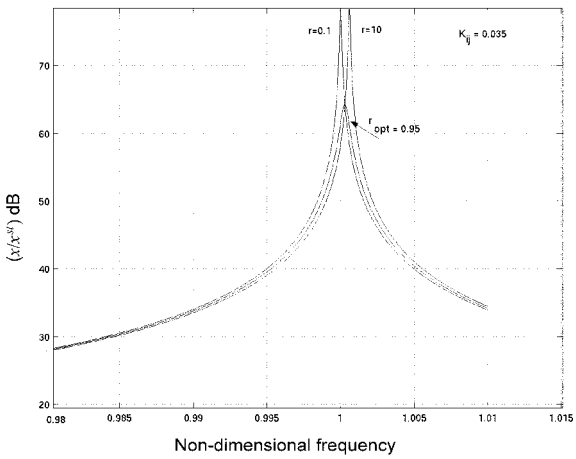

Fig. 11 Response of 1-DOF system with resistively shunted piezoelectric; $K_{ij} = 0.035$

The response of the 1-DOF system at various non-dimensional resistance values is shown in Fig. 10. The response is similar to that of a 1-DOF system with a linear viscoelastic solid in parallel as shown in Fig. 5. At optimal resistance, the peak of the transfer function is reduced due to the addition of damping, which is mainly attributed to the dissipation of energy across the resistance. The modal damping ratio can be found exactly by solving the roots of the cubic equation in the denominator of Eq. (38). The electromechanical coupling coefficient is mainly dependent on the system modal stiffness K and the piezoceramic stiffness K_{pzt}. The solution to the denominator of Eq. (38) gives the additive damping due to PZT. For a fixed value of non-dimensional resistance, r, the added damping mainly depends on K_{ij}. However, the experimentally evaluated value was found to be 0.035 following the procedure outlined by Hagood and von Flotow (1991, page 262). This large deviation is attributed to the effect of the bonding layer on the PZTs ability to transform mechanical energy into electrical energy. We now simulated the transfer function given by Eq. (38), fixing the value of $K_{ij} = 0.035$. The result is presented in Fig. 11. Note that the change in the resonance frequency is only about 0.001 Hz when the non-dimensional resistance is changed from 0.1 to 10. This confirms our experimental observation while performing the impulse hammer test, of no change in the resonance frequency with piezoceramic open- or short-circuited.

An experimental study of the effect of resistive shunting on vibration tip amplitude and added damping was carried out, and the results are shown in Figs. 12 and 13. In the case of variation in added damping with resistive shunting, Fig. 13, the experimental results match well with the analytical results, indicating that the assumptions made in the electro-mechanical modeling of the host beam and PZT with resistive shunting is quite accurate. Note that the additive damping as a function of non-dimensional resistance is similar to that of the variation of loss factor with frequency of a viscoelastic solid. However, in contrast to that of a viscoelastic material, piezo-resistive shunting is not prone to problems such as the ‘rubber to glass’ transition at a certain temperature that occur in most viscoelastic material used as vibration dampers. The experimental results for tip amplitude deflection as a function of resistance, Fig. 12, shows that the maximum reduction in tip deflection is about 4% at the optimum resistance value. The time-domain response of the beam with piezo short-circuited and piezo resistively shunted at the optimum resistance value

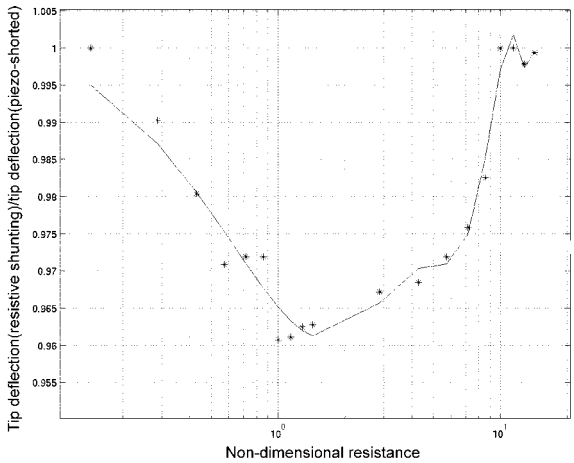

Fig. 12 Variation of tip amplitude as a function of resistance (Beam-I; Mode-I); Experiment

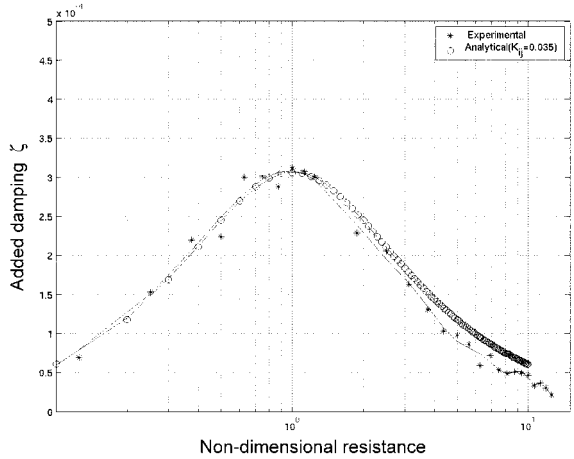

Fig. 13 Variation of additive damping as a function of resistance (Beam-I; Mode-I); Experiment and theory

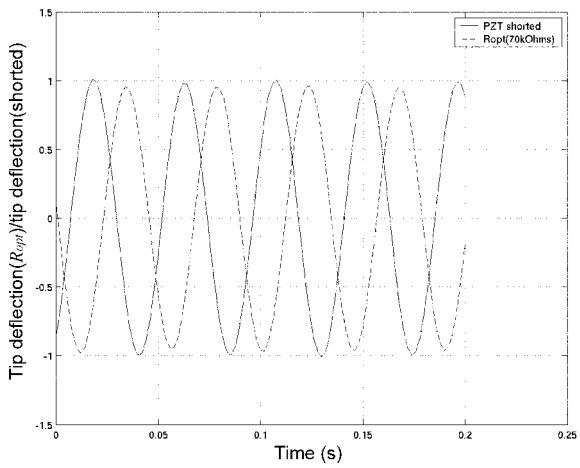

Fig. 14 Time domain response of beam with PZT (Beam-I; Mode 1)

is shown in Fig. 14.

Since the vibration reduction with resistive shunting was only around 4% for the first mode, we did not pursue to investigate the effect of resistive shunting on the second mode. Rather, we chose to investigate effect of form factors such as thickness ratio on piezo-resistive shunting.

4.2 Beam-II

Given the fact that the maximum electromechanical efficiency of the piezo alone, in the 1-3 direction, is at best 35%, resistive shunting is quite unlikely to significantly change the natural frequencies and enhance the damping. Of course, higher efficiencies can be realized when the piezo acts in a plane, k_p, or even in the 3-3 direction. Therefore, in order to maximize the effectiveness of

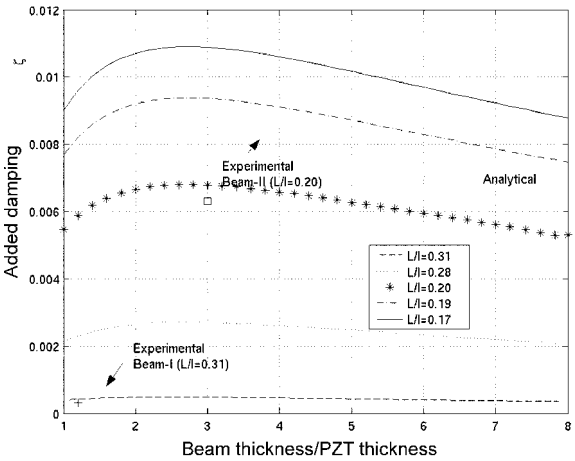

Fig. 15 Variation of added damping with thickness ratio(beam/PZT) for different beam length (l)/PZT length (L) ratios

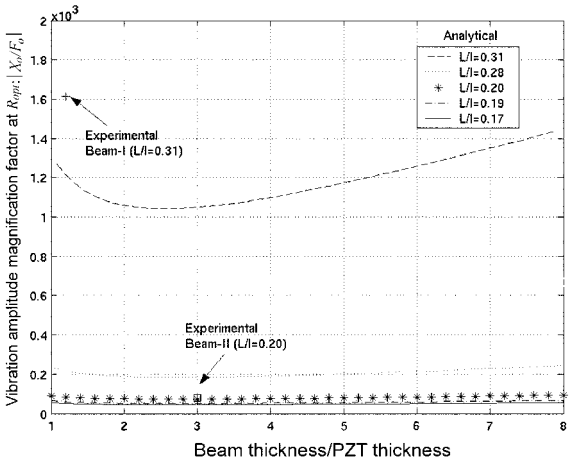

Fig. 16 Variation of vibration amplitude with thickness ratio (beam/PZT) for different beam length (l)/ PZT length (L) ratios

the piezoceramic shunting on the dynamics of the host beam structure, a study of the effect on added damping due to purely structural factors such as thickness ratio of beam to that of piezoceramic, and the length ratio of beam to that of piezoceramic, was carried out. The results of these investigations are presented in Figs. 15 and 16. Fig. 15 shows that the relative thickness values of the host beam and PZT, as well as their relative lengths, have an important influence on the added damping due to resistive shunting. However, for a given ratio of piezoceramic length to beam length, the added damping is a maximum at a thickness ratio of around 2.72. Above this thickness ratio, the added damping decreases. This is in-spite of the fact that increasing the beam thickness should increase the strain induced in the piezoceramic and thereby the added damping due to resistive shunting. However, the additive damping factor is really the ratio of the damping force to the product of the inertia and restoring forces. Increasing the beam thickness till some point induces greater strain in the piezoceramic, but beyond this thickness, the induced damping due to resistively shunted strain actuated piezoceramic is counteracted by the increase in inertia and stiffness due to a thicker beam. Therefore, the damping factor decreases with increase in thickness ratio beyond the value 2.72. Fig. 16 shows the resulting variation in the vibration amplitude of the beam with PZT resistively shunted at optimum resistance value. It is assumed in the numerical simulation that the beam with piezo short-circuited is has no damping. This is assumed to be the baseline configuration. The graphs clearly show the amplitude reduction as a function of thickness. At a thickness ratio of 2.72, the vibration amplitude, for a given length ratio, shows a minima. This is as it should be, as the added damping due to resistive shunting of the piezo is maximum at this value. The experimental results also show good agreement.

Based on the above results, we conducted experiments on another duralumin beam specimen with piezo bonded to it as shown in Fig. 7. This beam dimensions, henceforth referred to as Beam-II, were 250 mm long, 26 mm wide and 1.5 mm thick. The piezo-beam thickness ratio works out to approximately 3. Note that the added damping in this case was almost twice that of the Beam-I configuration. We conducted experiments to study the effect of resistive shunting on reducing the amplitude for two modes of the system. For the first mode, the variation of amplitude of response

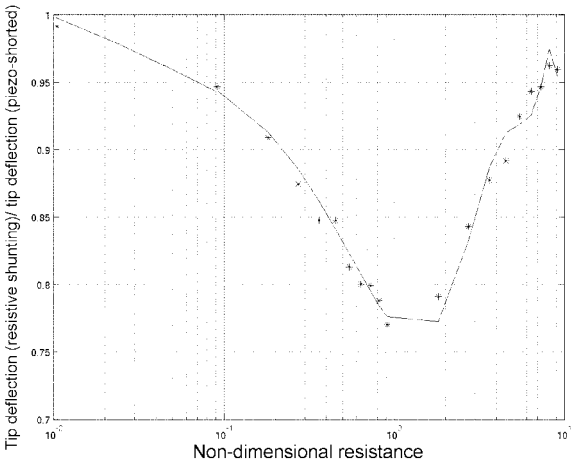

Fig. 17 Variation of tip amplitude as a function of resistance (Beam-II; Mode 1); Experiment

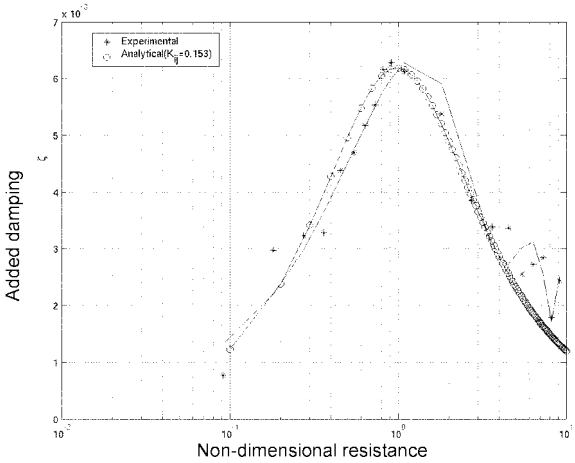

Fig. 18 Variation of additive damping as a function of resistance (Beam-II; Mode 1); Experiment and theory

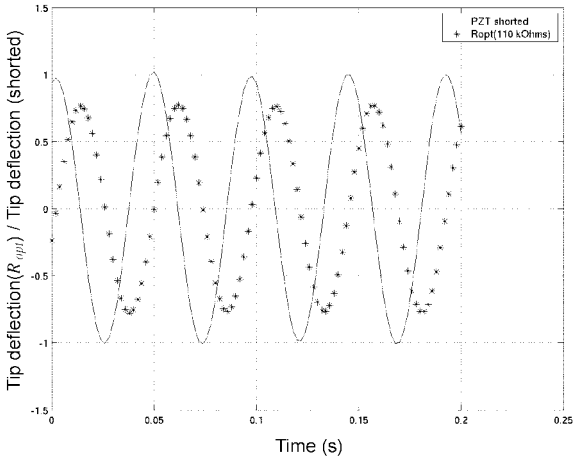

Fig. 19 Time domain response of beam with PZT (Beam-II; Mode 1)

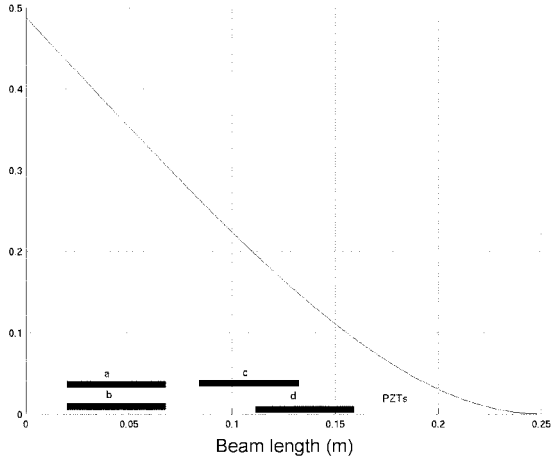

Fig. 20 Strain mode shape of Beam-II for first mode

and added damping as a function of resistance are shown in Figs. 17 and 18. Note that the maximum reduction in tip amplitude at a resistance value is around 23%. The added damping shows an increase of 60%. The time-domain response of the beam with piezo short-circuited and piezo resistively shunted at the optimum resistance value is shown in Fig. 19. It is illustrative at this point to plot the strain mode shape of the beam with piezo bonded onto it as shown in Fig. 20. Note that the maximum value of the strain in the first mode occurs at the root. So bonding the PZT close to the root will induce maximum strain in the piezo and consequently maximum voltage will be developed across the piezo. Of course, the electromechanical efficiency is governed by the k_{31} value that is approximately equal to 0.35 or 35% efficiency. In the present experiment we place the PZT as close to the root as possible taking into consideration space for leads and wires from the piezo to

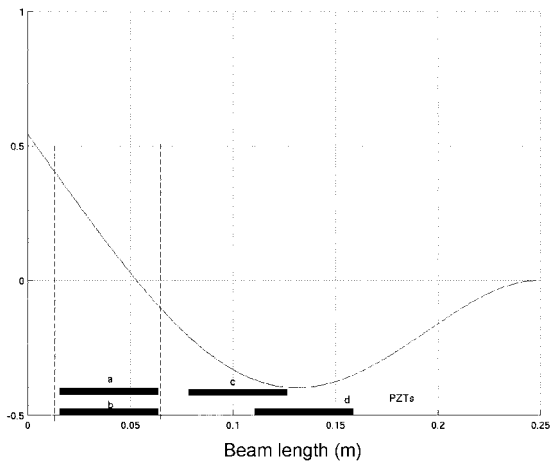

Fig. 21 Strain mode shape of Beam-II for second mode

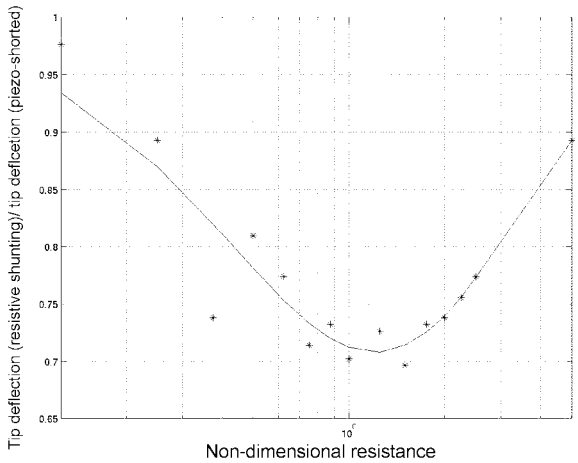

Fig. 22 Variation of tip amplitude as a function of resistance (Beam-II; Mode 2); Experiment

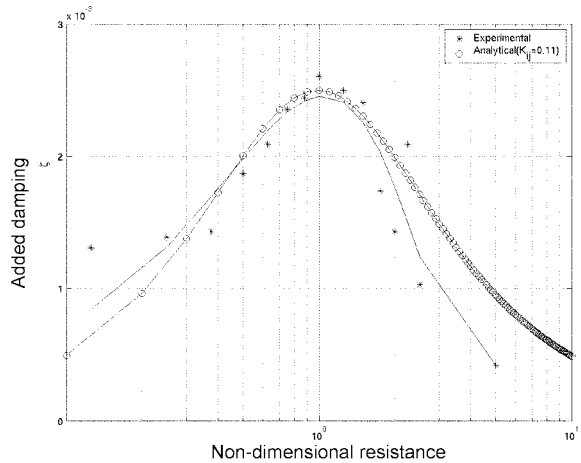

Fig. 23 Experimentally determined variation of additive damping as a function of resistance (Beam-II; Mode 1)

the resistance, etc.

For controlling the second mode of the beam we placed the piezo at a location close to the maximum value of the second strain mode shape as shown in Fig. 21. The variation of tip-amplitude of the beam and the added damping for the second mode as a function of resistance is shown in Figs. 22 and 23. The reduction in tip amplitude is 30% and increase in added damping is 50%. The time-domain response of the beam with piezo short-circuited and piezo resistively shunted at the optimum resistance value is shown in Fig. 24. Note that reduction in vibration amplitude is more in the second mode than in the first. This inspite of greater augmentation of damping due to resistive shunting in the first mode, which is 60%, than in the second mode, that is 50%. This is due to the fact that damping due to resistive shunting is viscous in nature and is proportional to the

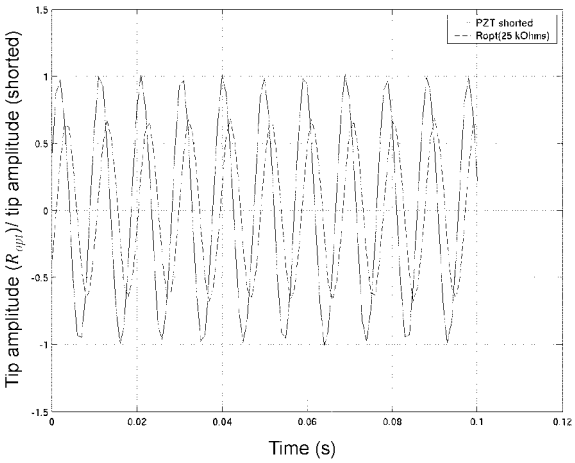

Fig. 24 Time domain response of beam with PZT (Beam-II; Mode 2)

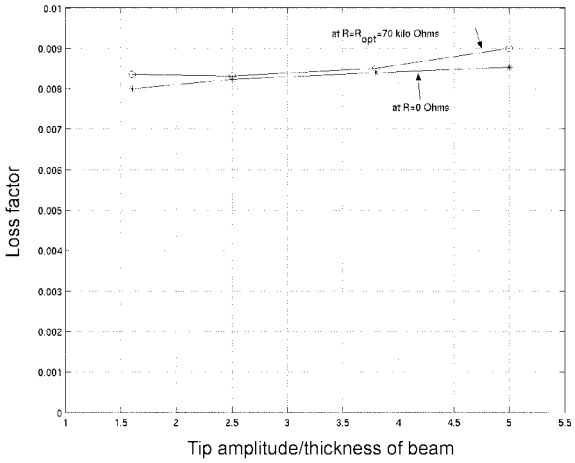

Fig. 25 Experimentally determined variation of loss factor with amplitude

frequency of vibration. Therefore higher modes are more easily damped.

Although additive damping due to resistive shunting behaves predictably along the lines of the linear theory derived above, we wished to investigate any deviation from linear behavior at relatively high amplitudes of vibration. In order to study the effect of vibration amplitude on damping, the loss factor at the optimum resistive shunting value is plotted as a function of amplitude in Fig. 25. Note that the loss factor is almost independent of amplitude pointing to the fact that the damping behavior of the resistively shunted piezoceramic structure is viscous in nature.

We also studied the effect of excitation frequency on the damping behavior of the resistively shunted piezoceramic. The excitation frequency was varied close to the first resonance frequency so that the beam-piezo dynamics could be modeled as a sdof system. We would like to point out that the vibration amplitude at off-resonance frequencies could not be kept at the level as at resonance since the forcing amplitude necessary to do so at off-resonance turns out to be very high. However, since we know that the loss factor does not change with amplitude, the variation of loss factor would only be a function of frequency. The loss factor variation is presented in Fig. 26. The variation of the loss factor with frequency is similar to that of a linear viscoelastic solid (Mallik 1990, Nashif *et al*. 1985). Also note the fact that the loss factor variation with frequency is similar to that of the variation of loss factor with resistance, since the non-dimensional resistance given in Eq. (32) or (39).

5. Conclusions

The effect of resistive shunting of a piezoceramic material bonded to a duralumin cantilever beam is investigated with reference to its vibration control effectiveness. Specifically, we have focused on the reduction of tip response amplitude, additive damping and change in resonance frequency for two modes of vibration of a cantilever beam. The studies on the added damping due to resistive shunting on a beam indicate the fact that the electro-mechanical coupling coefficient is an important

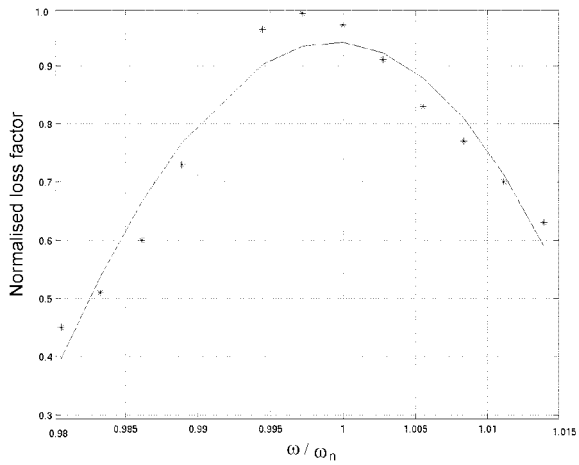

Fig. 26 Experimentally determined variation of loss factor with frequency of vibration

parameter. Higher values of k_{31} ensure better added damping and larger percentage change in natural frequency. We also investigated the effect of thickness ratio of the piezo with reference to the host beam structure on augmenting damping due to resistive shunting of the piezo. It is shown that for a given value of k_{31} and specified piezo length to beam length, there is an optimum thickness ratio at which damping due to resistive shunting is maximized. Vibration amplitude reduction of the order of 23% and 30%, respectively, for the first two modes of vibration were observed. The change in natural frequencies with resistive shunting of the piezoceramic was quite marginal.

We also experimentally investigated the effect of amplitude and frequency on the nature of damping. The loss factor was plotted as a function of measured tip amplitude of the beam for a fixed frequency of excitation. The results indicate that the loss factor is almost independent of amplitude, confirming that the damping behavior is predominantly viscous in nature. The variation of loss factor with damping too behaves as that of a linear viscoelastic solid modeled using spring-dashpot models. Experimental and analytical simulations are in close agreement.

Values of electromechanical coupling coefficient, k_{31}, are limited to a value of 0.35-0.36 with currently available piezos. However, for circular plates one can exploit the planar electromechanical coupling coefficient, k_p, whose values range between 0.65-0.70. The PZT should be in the form of a disc. Further, shear type piezoceramic actuators (here the poling direction is the 1 or 2 direction as opposed to the 3 direction in conventional piezos) higher electromechanical efficiencies of about 70% can be achieved. We plan to work with these types of actuators, and hope to present our results at a later date.

References

Crawley, E. and de Luis, J. (1987), "Use of piezoelectric actuators as elements of intelligent structures", *AIAA J.*, **25**(10), 1373-1385.

Davis, C. and Lesieutre, G. (1995), "Modal strain energy approach to the prediction of resistively shunted piezoceramic damping", *J. Sound Vib.*, **184**(1), 129-139.

Davis, C. and Lesieutre, G. (2000), "An actively tuned solid-state vibration absorber using capacitive shunting of

piezoelectric stiffness", *J. Sound Vib*., **232**(3), 601-617.
Hagood, N. and von Flotow, A. (1991), "Damping of structural vibrations with piezoelectric materials and passive electrical networks", *J. Sound Vib*., **146**(2), 243-268
Harris, C. (1996), *Shock and Vibration Handbook*, McGraw Hill Inc., New York.
Kandagal, S.B., Sarkar, S. and Venkatraman, K. (2000), "Passive vibration control using piezoceramic materials", Technical Report ARDB-SP-TR-2001-1020-1, Aeronautics Research and Development Board, New Delhi, India.
Mallik, A. (1990), *Principles of Vibration Control*. East-West Press Pvt. Ltd., New Delhi.
Nashif, A., Jones, D. and Henderson, J. (1985), *Vibration Damping*. John Wiley and Sons, New York.